Physics of Fluids

Flow dynamics in a variable-spacing, three bluff-body flowfield

Cite as: Phys. Fluids **30**, 025105 (2018); https://doi.org/10.1063/1.5001943
Submitted: 28 August 2017 . Accepted: 20 January 2018 . Published Online: 20 February 2018

M. Meehan, A. Tyagi, and J. O'Connor

COLLECTIONS

This paper was selected as an Editor's Pick

View Online Export Citation CrossMark

ARTICLES YOU MAY BE INTERESTED IN

Referee Acknowledgment for 2017
Physics of Fluids **30**, 010201 (2018); https://doi.org/10.1063/1.5022671

Optimum-wavelength forcing of a bluff body wake
Physics of Fluids **30**, 015101 (2018); https://doi.org/10.1063/1.4999091

Dependence of square cylinder wake on Reynolds number
Physics of Fluids **30**, 015102 (2018); https://doi.org/10.1063/1.4996945

Scilight Highlights of the best new research in the physical sciences
LEARN MORE!
AIP Publishing

AIP Publishing

© 2018 Author(s).

Flow dynamics in a variable-spacing, three bluff-body flowfield

M. Meehan, A. Tyagi, and J. O'Connor
Mechanical Engineering, The Pennsylvania State University, University Park, Pennsylvania 16802, USA

(Received 28 August 2017; accepted 20 January 2018; published online 20 February 2018)

This work explores the wake dynamics of systems with three bluff bodies with variable spacing. Studies of single-wake systems have shown that coherent wake vortices have a regular and predictable periodicity. A growing literature of dual-wake studies has shown that multi-wake systems are more stochastic than single-wake systems, and their dynamics are highly dependent on the spacing between the wakes. Here, we expand on this literature by investigating three-wake systems and find that the coherent dynamics of the wakes are highly intermittent. We use proper orthogonal decomposition to extract the most energetic modes of the three-wake system at six bluff-body spacings that span a range of dynamical "regimes." After describing the time-dependent behavior of the interacting wakes in these regimes, we use a statistical approach to describe the relative phase between oscillations in each of the wakes, identifying regimes where oscillations are more or less random. Interestingly, the wake oscillations are less random when the bluff bodies are positioned very close and relatively far from each other. In between these two extremes, an intermediary regime is identified where the wake oscillations are almost completely random; this finding parallels data from the dual-wake literature. Finally, we discuss the implications of the observed behaviors and possible future directions for this work. *Published by AIP Publishing.* https://doi.org/10.1063/1.5001943

I. INTRODUCTION

The goal of this paper is to characterize transitions in flow development and stability characteristics with variations in bluff-body spacing in a three bluff-body flowfield. The applications of this work are far reaching, from flame holders in jet engine augmentors, to air moving though power transmission lines, to flows through heat exchangers, to piers supporting trusses in unsteady waters. In each of these applications, adjacent flowfields, or a series of individual wakes, experience a significant level of interaction. The interaction can change both the time-averaged and dynamical characteristics of the interacting flowfield as compared to a single element of the flow field, such as a single jet or wake. In this work, we focus on changes to the time-averaged and large-scale dynamical features of planar flowfields with varying levels of interaction. We have chosen a Reynolds number regime that highlights key hydrodynamic stability features of a two-dimensional wake flow. However, it is likely that turbulence is not fully developed at these Reynolds number conditions. As such, we do not focus on the turbulent characteristics of the flowfield but rather the flow development and large-scale dynamics.

A. Literature review of development and stability of interacting flowfields

A review of the literature reveals that interacting flowfields have been studied for some canonical flows, especially plane jets and wakes. Interacting jets fall into two categories: unventilated jets, where a surface is placed between the jet exits, and ventilated jets, where there is no surface between jets and air is free to flow between the two nozzles.[1] The flowfield of these two configurations differs by the presence of a recirculation zone, which develops between the unventilated jets as a result of the low-pressure zone along the centerline of the jets. Comparison studies of these two configurations have shown that ventilated jets merge further downstream than unventilated jets because of the additional entrainment along the centerline.[2]

The flowfield of interacting plane jets is typically divided into three regions: the converging region, present in unventilated jets where the core flows and shear layers are separated by a recirculation zone; the merging region, where the shear layers begin to interact; and the combined region, where the two jets are indistinguishable. The converging region of plane jets shows significantly different characteristics from the initial development of a single jet in terms of the time-averaged flow trajectory, turbulence levels, and instability characteristics. This also implies that the development of the shear layers on either side of the jet, termed the "inner" and "outer" shear layers, can be influenced by the interaction. Ko and Lau[3] and Nasr and Lai[1] reported spectra of turbulent fluctuations in the inner and outer shear layers of two plane, unventilated jets. The results from Nasr and Lai are particularly interesting as they examined the effect that interaction has on hydrodynamic instability and the large-scale coherent structures produced by the instability. The development of the preferred shear layer mode at a frequency of approximately 2400 Hz was damped in the inner shear layer, as compared to the outer shear layer, as a result of interaction with the adjacent recirculation region. Additionally, the first subharmonic was almost entirely damped in the inner shear layer. As compared to the instability development in a single jet, the fluctuation spectra in the outer shear layer of the dual-jet configuration still showed damped oscillations, indicating that the interaction of the two jets affected even the outer shear layer development, despite the lack of direct interaction in the outer shear layers.

Evidence of periodic dynamics in pairs of interacting plane jets have been explored more thoroughly by both Bunderson and Smith[4] and Soong *et al.*[5] The experiment of Bunderson and Smith considered a Reynolds number of Re = 21 500 at a range of jet spacings and momentum ratios between the two jets. The two jets displayed strong oscillatory motion, including side-to-side flapping and formation of large coherent structures, when the momentum ratios were matched over a range of jet spacings. Similar flapping and coherent structure formation were noted by Soong *et al.*[5] at much lower Reynolds numbers, Re = 60-200, in a direct numerical simulation (DNS) calculation. However, the work by Soong *et al.* showed that as Reynolds number increased above Re = 80, the oscillations became chaotic as opposed to periodic. The impact of turbulence on this chaotic behavior is not known, as the simulation remained in the laminar regime.

Limited data show the impact of jet spacing on the downstream development of interacting plane jets. Tanaka[6–8] showed that the development of the unventilated interacting jets bifurcated as a function of the jet separation, D, divided by the jet width, a. This trend was quantified by tracking the location of the stagnation point at the downstream end of the recirculation region as a function of D/a; for $D/a > 16$, the downstream location of the stagnation point varies more quickly with jet separation. The authors point to the differences in the static pressure fields and resultant entrainment in these two regimes as the driving reason behind this changing trend. However, this result may not be universal and is likely not the same in ventilated jets because of the lack of the central recirculation region. It is clear from the literature of interacting jets that the jet development in interacting jets is fundamentally different than that of single jets in terms of the mean velocity profiles, turbulence development, and hydrodynamic instability. These differences are significant enough to put "interacting jets" into a separate category from single jets, and possibly, that "dual-jet" systems are different from systems with more jets as a result of the interaction between the inner and outer shear layers. In general, *the development of interacting jet flows cannot be deduced from the single flow behavior*.

The interacting wake literature heavily focuses on the wake behind pairs of bluff bodies, including circular cylinders, square cylinders, and flat plates. Beginning with investigations by Biermann and Herrnstein[9] in 1933 and Spivack[10] in 1946, researchers noted that the drag coefficients on side-by-side bodies had two curious features. First, the flow appeared to be bi-stable; at a given Reynolds number and spacing, the drag coefficients "flip-flopped" between two values. Second, the average of these two drag coefficients was typically lower than the drag coefficient on a single cylinder, indicating significant interaction in dual-body systems. Many studies investigated the reasons for this bi-stable behavior in dual-wake systems, including the work of Sumner *et al.*,[11] Le Gal and co-workers,[12,13] Kiya *et al.*,[14] Yen and Liu,[15] Kim and Durbin,[16] Bearman and Wadcock,[17] Wang and Zhou,[18] Carini *et al.*,[19–21] and Hayashi *et al.*[22] While the Reynolds numbers (based on diameter) of these studies vary widely, from the laminar (Re = 30) to fully turbulent (Re = 47 000) flow, most studies pointed to ranges of bluff-body spacings that resulted in different wake structures, including the Bérnard von Kármán (BVK) instability, and dynamics. Table I provides an overview of these ranges, where w is the center-to-center spacing of the bluff bodies and D is the diameter of the bluff bodies. It should be noted that many of these studies used the non-dimensional parameter s/D for spacing, where s is the gap width between the two bluff bodies; despite this difference, the results are typically the same. Alam *et al.*[23] also noted that the ranges for different bluff body shapes were slightly different, particularly in the transition regime, but followed the same general progression.

There are several key features of these ranges. First, in the range of $1.3 < w/D < 2.2$, the "gap flow," or flow between the two bluff bodies, is "biased" and preferentially angles to one side. Mizushima and co-workers[24–26] found that this biased structure exists in up to as many as 14 wakes at low Reynolds numbers (Re = 23-30); this alternating wake structure was also seen in three-wake systems by Sumner *et al.*[11] at Re = 500-3000 and more recent work by Zheng and Alam[27] at Re = 150, although no data exist at higher Reynolds numbers to confirm that this trend continues for more than two bluff bodies. In the dual-wake system, the wakes "flip-flop," or change bias, in this same range of spacings. Experiments by Kim and Durbin[16] at Re = 3000 showed that this flip-flop process is random and fits to a Poisson distribution, as did experiments by Bearman and Wadcock[17] at Re = 25 000. Wang and Zhou[18] used high-speed LIF imaging to show the mechanism for the flip-flop, indicating that vortices from the wider wake were entrained into the narrower wake when phase lag in the vortex shedding in the wider wake allowed those structures to be more easily entrained. Over the course of three to four vortex shedding periods, this entrainment of fluid builds up, eventually causing the narrow wake to overtake the wider wake, and the

TABLE I. Overview of the dual-body wake structure and dynamics. w/D ranges taken from Ref. 23, although these are representative of the literature.

Spacing	Wake structure	Wake dynamics
$w/D < 1.3$	Single-wake structure and symmetric	Asymmetric vortex shedding from the BVK instability
$1.3 < w/D < 2.2$	Biased gap flow with one narrow, one flared wake; flip-flopping of the wake structure	BVK shedding from each bluff body at different frequencies and wakes shed out-of-phase
$2.2 < w/D < 3$	Some bias	Transition regime with significant intermittency in the wake shedding phase
$3 < w/D < 4.6$	Unbiased wake structure	Out-of-phase BVK vortex shedding on each bluff body
$w/D > 4.6$	Unbiased wake structure	Weakly coupled shedding or in some cases, no coupling

system "flips." Linear stability analysis by Carini *et al.*[20] at much lower Reynolds numbers, Re = 50-90, showed that this flipping process is not random but instead is driven by a secondary instability in the flowfield. The authors were careful to note that this result may not apply at higher Reynolds numbers. However, their structural sensitivity analysis[21] showed that the flipping is driven by the structure of the shear layers near the bluff body; these findings aligned well with experimental findings at Re = 3300 by Kim and Durbin,[16] who found that acoustic forcing of the shear layers could suppress the bias and the flipping. Additionally, they found that other bluff-body shapes, like squares and flat plates, where the shear layer separation location is not variable, as it is on a circular cylinder, did not see intermittent flipping; this was confirmed by Hayashi *et al.*[22] in wakes behind flat plates at Reynolds numbers from Re = 6000-19 000.

As the spacing increases, the bias between the two wakes decreases and the interaction between the bluff body shear layers reduces. Many studies noted significant intermittency in vortex shedding frequency and phase between the two bluff bodies in these intermediate regions. In particular, multiple studies, reviewed by Zdravkovich[28] in 1977, indicated that the behavior of the dual-wake system in the range of $2.2 < w/D < 3$ is highly sensitive to the spacing, Reynolds number, and bluff-body shape. Beyond this point, studies noted some lock-in between vortex shedding, although results between studies start to diverge significantly beyond $w/D > 4$. This is likely a result of differences in Reynolds numbers in the available literature.

Few studies consider the dynamics of multi-wake systems with more than two wakes. Sumner *et al.*[11] investigated both two- and three-wake systems using circular cylinders at Reynolds numbers between Re = 500-3000, and Hayashi *et al.*[22] considered systems of two, three, four, and five flat plates at Reynolds numbers between Re = 6000-19 000. While Sumner *et al.* showed some similarities in the dynamics of the two- and three-wake systems, Hayashi *et al.* mostly focus on the structure of the flow rather than the dynamics. Recent work by Zheng and Alam[27] identified behavioral regimes for three-wake systems at Re = 150 using DNS, focusing on significant variations in the lift-coefficient as a function of spacing as a metric for the global flow behavior. As a result of the dearth of data on three-wake systems, *we hesitate to draw any conclusions about multi-wake systems from the findings in dual-wake systems.* It is also clear from the dual-wake literature that interaction between the shear layers formed along the free-stream side of the bluff bodies and those formed in between the bluff bodies plays a critical role in determining the dynamics of the two-wake system. This is particularly true at close spacings, where the bias in the flow is strongly driven by this interaction. In systems with three or more bluff bodies, the interaction between the free stream and the interaction shear layers will not exist for the "inner" flows, changing the flow interaction significantly.

B. Scope of this study

This review of the literature indicates that there are several unanswered questions about the development and stability of interacting flowfields. We have scoped this study to address two critical gaps in the current literature. First, we add to the very small quantity of data on more than two interacting wakes. Second, we focus on the large-scale dynamics of these flowfields, which can influence both large-scale and small-scale processes in technologies with interacting flows. The presence of coherent structures has been shown to enhance mixing on a local scale,[29] while large-scale dynamics can significantly impact system performance; in combustors, large-scale structures drive limiting processes such as blow-off[30] and combustion instability,[31] and in structural configurations, large-scale motions can drive high-cycle fatigue. In particular, we are interested in the variations in frequency and symmetry of these dynamics. We use a number of analysis techniques to extract and analyze the coherent dynamics of the flow at varying levels of interaction.

In this study, we limit ourselves to planar flowfields in a particular Reynolds number range. We chose a planar flowfield for two main reasons. First, the majority of the literature on interacting jets and wakes in general focuses on planar configurations; this historical data provide important context for the current study. Second, the target technology of our facility is bluff-body stabilized flames, as in jet engine augmentors[32] or furnaces and heaters.[33,34] Our initial reacting studies in this facility indicated that flow interaction has a first-order effect on flame development;[35] as such, the present study is motivated by a need to understand the development and stability of interacting flows at varying levels of interaction.

We have chosen the Reynolds number range, where the Reynolds number is defined based on bulk flow velocity (bulk flow velocity is defined as the mass flow rate divided by the density of the fluid multiplied by the open area of the top of the experiment) and bluff-body diameter, $Re = \bar{u}D/\nu$, for this study for two reasons. First, it corresponds with the Reynolds numbers of the reacting flow studies that preceded it.[35] More importantly, though, it represents an important range of Reynolds numbers in the stability of wake flows. At $Re < O(100)$, the wake flow is entirely laminar and only small asymmetric disturbances are present. Near $Re = O(100)$, the von Kármán vortex street is formed in the wake, the result of a global instability in the wake flow. In this low Reynolds number regime, Williamson proposed the wake shedding Strouhal number scales with Re as $St = -3.3265/Re + 0.1816 + (1.6 \times 10^{-4})Re$,[36] but above a Reynolds number of approximately $Re = O(1000)$, the Strouhal number is invariant with Re and is equal to approximately St = 0.2-0.3 for circular bluff bodies.[37] While the vortex shedding coherence decreases with increases in the Reynolds number, and hence turbulence intensity, the general structure of the single wake remains the same until $Re \approx 200\,000$.[38] A bifurcation takes place near Re = 1000,[38] where both the shear layer and wake instabilities are present. The presence of both modes of instability is important for understanding the impact of interaction on the stability of the flow. Above this Reynolds number cutoff, both the shear layer and wake instabilities are still present, but increasing the Reynolds number also increases the turbulence intensity, particularly in the shear layers. Stronger turbulent motions reduce the coherence of large-scale vortical structures, generated by the shear layer and wake instabilities. In order to preserve the integrity of these structures but still capture key

instability characteristics present in Reynolds numbers greater than $Re = 1000$, we have chosen to operate at $Re = 4000$.

II. EXPERIMENTAL DESCRIPTION

A. Experimental facility

This experiment consists of a duct that is 36 in. (914.4 mm) tall and has an exit dimension of 12×4 in. (304.8×101.6 mm). Bluff bodies are placed at the outlet of this duct and are affixed to the experiment on tracks so that their position at the exit can be varied. Dry air at ambient temperature is mixed with aluminum oxide tracer particles from a vortex particle seeder and used for particle image velocimetry (PIV). Inside the duct, the mixture passes through two 4 in. (101.6 mm) thick plastic honeycombs, both with 0.125 in. (3.18 mm) cell diameter, to ensure uniform flow. A perforated plate, 0.0468 in. (1.19 mm) thick and 0.125 in. (3.18 mm) cell diameter, is placed 6 in. (152.4 mm) below the top surface of the experiment for turbulence generation. The resulting turbulence intensity at the bluff bodies is ~3%. A schematic of this configuration can be seen in Fig. 1. This experiment was designed following that of Shanbhogue,[39] who studied the dynamics of single-wake flows and flames; the single-wake configuration in this study mimics conditions from Shanbhogue's previous work. The goal of the reacting experiments, not discussed here, was to understand the role of flame interaction on flame dynamics and compare these results to the large body of experimental work by Shanbhogue and complementary theoretical work by Shin.[40] It was quickly recognized, though, that the dynamics of the interacting flames were largely driven by the dynamics of the interacting flows, which is the focus of the current work.

The facility generates wake flows in various arrangements that include a combination of three bluff bodies and two top plates, as shown in Fig. 1(a). Each bluff body is a stainless steel, triangular prism with equal side lengths of 0.75 in. (19.05 mm) and length of 4 in. (101.6 mm). They are anchored with clamps on the outside of the front and back of the experiment. The clamps are comprised of a seat in which the bluff body is placed and a 0.125 in. (3.18 mm) thick plate with counter-bored bolts that is placed on top of the bluff body to secure it to the seat. This mounting device barely protrudes above the top surface of the bluff body and, as such, is not expected to significantly impact the flow. The top plates are used to restrict the flow on the edges of the experiment and are rectangular with dimensions 6.25×5 in. (158.75×127 mm) and a width of 0.5 in. (12.7 mm). The top half of the edge closest to the bluff bodies and in contact with the flow makes an angle of 60° relative to the direction of the flow [see Fig. 1(a)], identical to the bluff bodies. A through-hole allows a bolt to pass through the plate and then tighten to the flanges on the left and right of the flow facility. Once all objects are secured, they create a flush, top surface of the experiment at $x = 0$, where x is defined as the axial direction and y as the cross-stream direction.

The various arrangements used in the study include a single bluff body and three bluff bodies. The single bluff-body case has the equilateral triangular bluff body placed at the center of the viewing window, and the top plates are moved sufficiently far away to not influence the flow pattern; the open dimension of the duct exit at this condition, created by the placement of the top plates, is 4×4 in. (101.6×101.6 mm), like that of Shanbhogue.[39] In the three bluff-body configuration, each bluff body is placed on either side of the central bluff body. The center-to-center measurement between bluff bodies, shown as w in Fig. 1(a), is equal on both sides, and $s = w - D$ for the spacing between bluff bodies. Due to the width of the clamps holding the bluff bodies, the minimum center-to-center measurement is $w = 32$ mm. In the three bluff-body configuration, the open area between bluff bodies and between a bluff body and a top plate is equal as well. For simplicity in further discussions, the bluff bodies are labeled as wake 1, wake 2, and wake 3 for the left, central, and right bluff bodies, respectively, as shown in Fig. 1(a).

B. Diagnostics

High-speed PIV is used to obtain axial (x-direction) and transverse (y-direction) velocity data. The laser (Quantronix Hawk-Duo 532 nm Nd:YAG dual cavity laser) outputs light with a wavelength of 532 nm and with a total pulse energy of 10 mJ at 4 kHz, with a pulse width of 190 ns. The beam passes through a collection of sheet-forming optics to form a diverging sheet on top of the experiment. The laser sheet illuminates the aluminum oxide tracer particles, approximately 0.5-2.0 μm in diameter. A Photron FASTCAM SA5 at full 1024×1024 resolution fitted with a CarlZeiss Makro-Planar

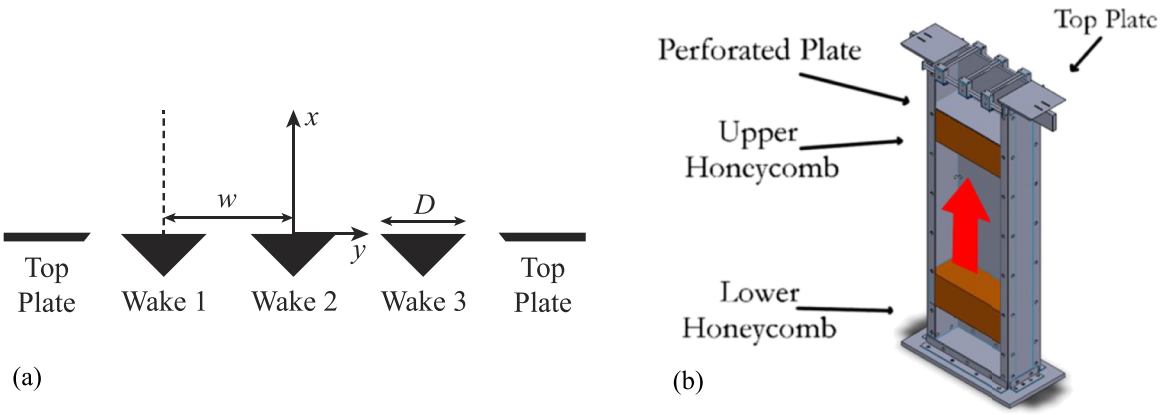

FIG. 1. Schematic (a) and drawing (b) of experimental configuration (front plate removed to show flow conditioning).

100 mm lens and 14 mm extension tube records images and velocity data through a 532 nm bandpass filter. The resulting spatial resolution is 0.129 mm.

PIV calculations were performed using DaVis 8.3 from LaVision. For each case, 5001 images are acquired at a data acquisition rate of 4 kHz. The raw seeded images are first preprocessed using a five-frame sliding minimum filter. The vector fields are calculated by using a multi-pass algorithm where the first pass is performed with an interrogation window size of 64×64 and 50% overlap while the final two passes are performed with a 16×16 window size with 50% overlap. This results in a vector resolution of 1.0 mm. Post-processing of vectors in DaVis includes a universal outlier detection scheme with a 3× median filter. This ensures removal of groups with less than 5 vectors and vectors with a residual greater than 2. It also ensures re-insertion of vectors with a residual less than 3. The average number of vectors replaced per dataset range from 5% to less than 7%, and the percent first choice vectors are between 88% and 93% for the datasets analyzed in this paper. This processing results in an average PIV uncertainty of approximately 10%-15% of the bulk flow velocity and a root mean square (RMS) PIV uncertainty of 9%-13% of the bulk flow velocity in the regions of interest for this study. Specific numbers varied case by cases and can be found in the Appendix.

C. Analysis methods

1. Frequency spectra

The frequency spectra of velocity signals are calculated to understand the spectral content of the velocity field. Spectra are calculated in two ways. First, a single-sized fast Fourier transform (FFT) is used and the power spectral density (PSD) is calculated to identify peaks in the spectra. Some of the PIV datasets included frames that were significantly corrupted; this issue was not discovered until much after the experiment was run. As a result, we used a Lomb-Scargle method[41] for constructing PSDs from signals that have missing samples; this method was only needed on data sets: $w/D = 2.20$ and $w/D = 2.47$. The frequency is reported as a Strouhal number, $St = fL/U$, where f is the frequency (in Hertz), L is a length scale relevant to the oscillations, and U is a velocity scale. In this study, the bluff-body diameter is used as the length scale, and the bulk flow velocity is used as the velocity scale.

2. Proper orthogonal decomposition

Proper Orthogonal Decomposition (POD) provides insight into the flow development by finding the large-scale dynamics in the modes containing more energy. Since the POD is an energy-based decomposition, it is ideal for identifying the differences in large- and small-scale structures in the context of turbulent flows. Here, the POD provides a basis set that maximizes the turbulent kinetic energy, as calculated by two components of velocity in this two-dimensional measurement. This is done by solving an eigenvalue problem on the two-point correlation tensor of the velocity field. The details of the POD can be found in the work of Berkooz *et al.*[42] This study uses reconstructed velocity fields from the highest-energy POD modes to remove turbulence and other small scale-dynamics and better understand intermittency in the wake motions.

TABLE II. Test matrix with bluff-body spacings in mm.

Spacing (mm)	32	37	42	47	52	57	Single wake
w/D	1.68	1.94	2.20	2.47	2.73	2.99	n/a
s/D	0.68	0.94	1.20	1.47	1.73	1.99	n/a

3. Constructing an analytic signal

To quantify the time-dependent behavior of signals with varying frequency and phase, a complex analytic signal is constructed from the original real-valued velocity signal. Having the analytic signal allows for extraction of the approximate phase and frequency at any given time in the signal. Gabor[43] proposed two methods for generating a unique complex signal, suppressing the amplitudes with negative frequencies outputted from a Fourier transform and adding the real-valued signal to the Hilbert transform of the signal multiple by the imaginary unit. He then showed that these two procedures were equivalent. For this study, the analytic signal $z(t)$ was constructed by applying the Hilbert transform $H[s(t)]$ to the real-valued signal $s(t)$ such that $z(t) = s(t) + jH[s(t)]$. This quantity was computed in MATLAB using the built-in function *hilbert*(). From there, the instantaneous frequency and phase could be extracted and interpreted by taking the inverse tangent between the real and complex values of the analytic signal.[44] While the instantaneous frequency and phase are mathematical constructs, they provide critical information about the behavior of periodic, yet intermittent, systems. This technique is used to study the interacting wakes generated by multiple bluff bodies.

4. Test matrix

Seven different arrangements were used in this study: six cases with three bluff bodies and one case with a single bluff body, the latter being considered the single element "unit flow" to establish a baseline for the interacting cases and ensure our data are consistent with other experiments. For this investigation, the center-to-center spacing w was increased in 5 mm increments, a resolution that seemed sufficient based on previous experimental investigations, from the experimental minimum and maximum. Table II outlines the seven test cases along with their corresponding w/D and s/D values.

III. RESULTS

A. Variations in time-averaged flow topology

Understanding the time-averaged flow topology allows us to better describe the dynamical features of the flow. Figure 2 shows the time-averaged axial velocities with streamlines for each of the seven cases; w/D is labeled above each image. In the single bluff-body case, shown as the top left image, a recirculation zone is present downstream of the bluff-body and extends approximately 2-3 bluff-body diameters downstream. The structure of the flow is very similar to previous studies of this canonical geometry.[38]

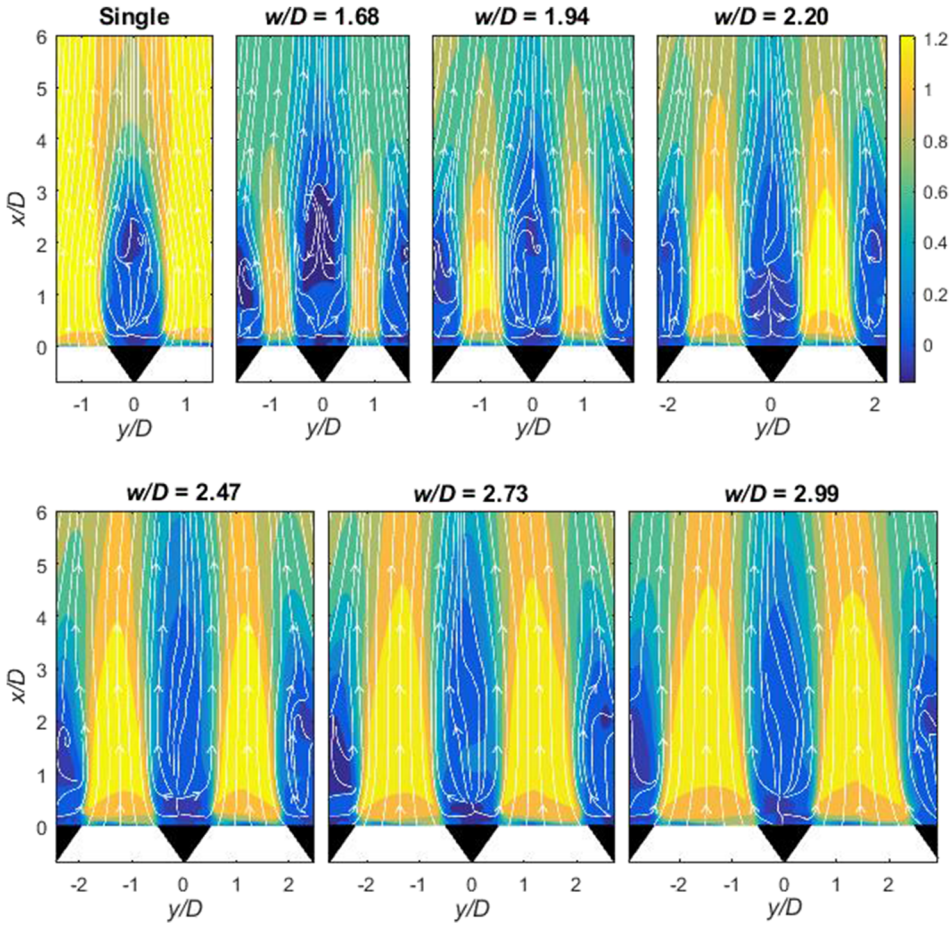

FIG. 2. Time-averaged axial velocity with streamlines.

The presence of multiple bluff bodies changes the time-averaged flow characteristics as compared to the single bluff-body flow. At the smallest spacing for interacting bluff bodies, w/D = 1.68, the streamlines emerging from the flow around the central bluff body, also referred to as the "jets," first diverge until approximately x/D = 2.5 and then converge farther downstream. In investigations with three bluff bodies, Sumner *et al.*[11] found a biased flow pattern for a similar w/D to this condition. In their study, the wake from the center was typically larger and dominated the wakes on either side, forcing the center jet flows to be biased away from the center wake. Farther downstream, all four "jets" begin to merge together. This merging has been seen in interacting plane jets, where closely spaced jets will deflect inwards toward the centerline of the flow.[1] This convergence can be seen to a lesser extent at all bluff-body spacings; as a result, the recirculation zones in wakes 1 and 3 are asymmetric about the centerline of the bluff body.

Another interesting aspect of the time-averaged flow is the change in recirculation zone strength and size behind the bluff bodies at different spacings. The backflow velocity in the center recirculation zone is highest at close spacings (w/D = 1.68) and then weakens as the spacing between bluff-bodies increases. At w/D = 2.47 and larger spacings, the center wake region contains almost no time-averaged recirculating flow, although recirculation is present on an instantaneous basis. The region of velocity deficit extends farther downstream than in the closely spaced cases, which reduces the merging of jets on either side of the center bluff body. The recirculation zones behind wakes 1 and 3, however, contain time-averaged recirculation for all spacings and have stronger recirculation than that of wake 2 at all spacings. This is likely the result of the quiescent ambient boundary condition on the edge of the experiment, which promotes more shear between the outer "jets" than a free-stream boundary condition would. It is also interesting to note that the structure of the recirculation zones for wakes 1 and 3 is different than that of wake 2; they deform inward toward the flow centerline starting at approximately x/D = 1.5 in all cases, and the extent of velocity deficit downstream is shorter than that in wake 2.

The changing time-averaged structure of the flowfield with bluff-body spacing has a significant impact on the fluctuating components of the velocity field. Figure 3 shows the root mean squared (RMS) velocity fluctuations of both the axial and cross-stream velocity components for the single wake and three-wake systems at various spacings. As expected, the highest RMS value for the single bluff body occurs in the wake at approximately x/D = 2.5-4 because this is where the von Kármán vortex street is the most pronounced. The von Kármán vortex street is a strong, coherent oscillation that drives significant fluctuation energy in the flowfield, increasing the RMS in the wake region. There is also significant fluctuating energy in the shear layers upstream of the wake region caused by the Kelvin-Helmholtz (KH) instability.[45]

The RMS velocity distributions are significantly different in the three-wake systems than in the single-wake system. In general, the RMS values are lower, a result of the loss of coherence of the wake vortex shedding mode. At the smallest

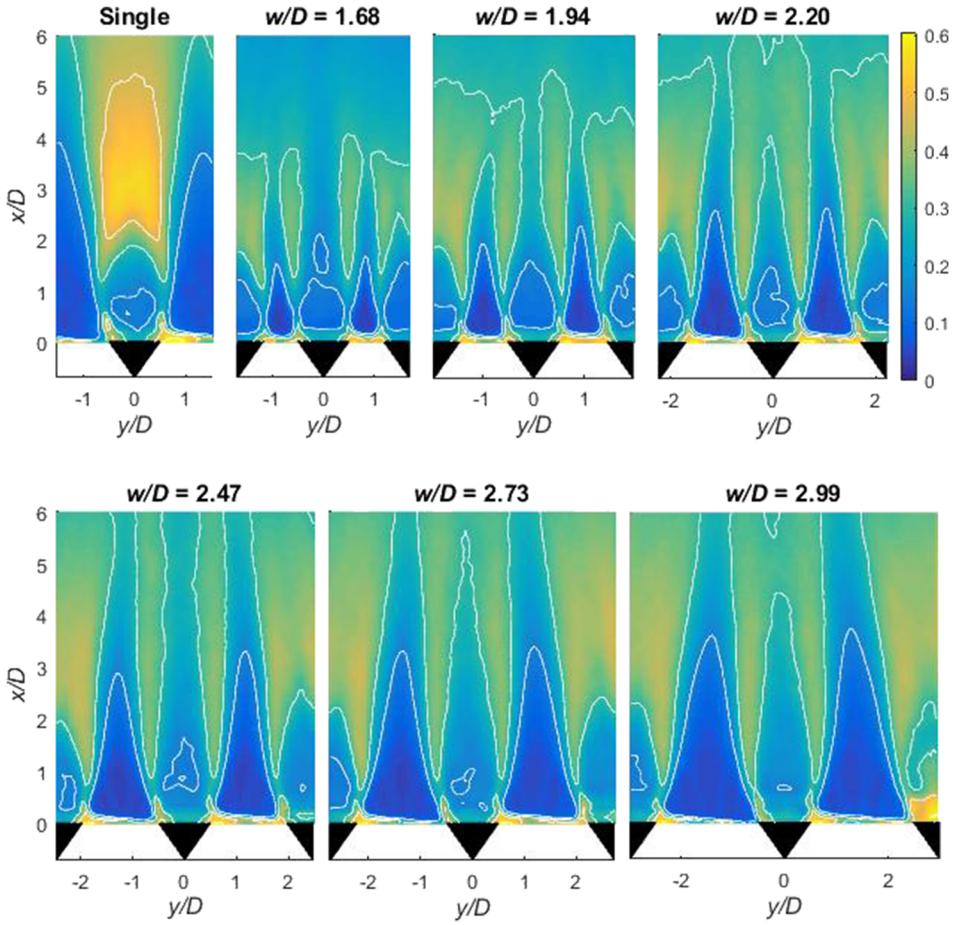

FIG. 3. RMS velocity fluctuations with white contours at $u_{rms}/\bar{u}$ increments of 0.5 over the range of $u_{rms}/\bar{u} = 0 - 2.5$.

spacing of $w/D = 1.68$, the RMS value is highest at $x/D = 1.5$-3.5 along each shear layer, rather than the wake centerline, and quickly decreases downstream. As the bluff-body spacing increases, the RMS value increases in both the shear layers and in the wake region for all three wakes. For spacings of $w/D = 2.20$ and above, the RMS structure in wake 2 is different than that in the outer wakes, wakes 1 and 3. In particular, RMS fluctuations are still concentrated in the shear layers for wake 2, while a higher RMS value is present along the wake centerlines for wakes 1 and 3. The dynamical features that cause this difference are analyzed in Secs. III B 2–III B 3.

Cuts of the time-averaged axial velocity and total RMS velocity fluctuations at three downstream distances—$x/D = 0.5, 3$, and 5—are shown in Fig. 4. The cross-stream coordinate has been non-dimensionalized by s, allowing for direct comparison of the flow profiles at the shear layers and in the wakes at the exit. At $x/D = 0.5$, the time-averaged velocity profiles show that the inlet conditions for all of the multiple bluff-body cases have very similar inlet profiles. Similarly, the total RMS inlet profiles for these interacting cases peak at approximately the same y/s location, where the KH instability dominates, and the total RMS levels in the shear layers are relatively similar for all cases. There are small differences in the RMS values in the wake region, however, where the two closest spacings of $w/D = 1.68$ and 1.94 have the lowest total RMS values as compared to the larger spacing cases. The similarity of the time-averaged and total RMS profiles near the inlet of the experiment for all the spacing cases suggests that the differences in wake behavior further downstream are not the result of significant differences at the inlet to the experiment.

At $x/D = 3$, the peak RMS values increase slightly with increasing spacing, with $w/D = 1.68$ having the lowest RMS and $w/D = 2.99$ having the highest values in the shear layers, although differences in flow merging between the spacing cases change the location of the shear layers in s/D space. At $x/D = 5$, there is a noticeable transition in the RMS profiles from $w/D = 1.68$ to $w/D = 2.20$. At $w/D = 1.68$ and 1.94, the RMS profiles are relatively flat, indicating that the three wake flows have merged by this point. At $w/D = 2.20$ and above, the shear layers are still present, although the peak RMS values at this downstream distance are very similar for all cases.

B. Variations in coherent dynamics

1. Dynamics of single flows

Before discussing the dynamics of interacting flows, it is useful to provide a baseline configuration; in this case, we consider the well-established dynamics of a single wake flow. Single wake flows in this Reynolds number regime are known to display vortex shedding in both the shear layer and wake, where the Kelvin-Helmholtz instability in the shear layer is known to have characteristic frequencies near $St = fL/u_o = 0.017$,[46] and the Bérnard von Kármán instability in the wake is known to have characteristic frequencies near $St = fD/u_o = 0.2$–0.3.[38] A frequency analysis of the fluctuating cross-stream velocity component along the shear layers in the single-wake

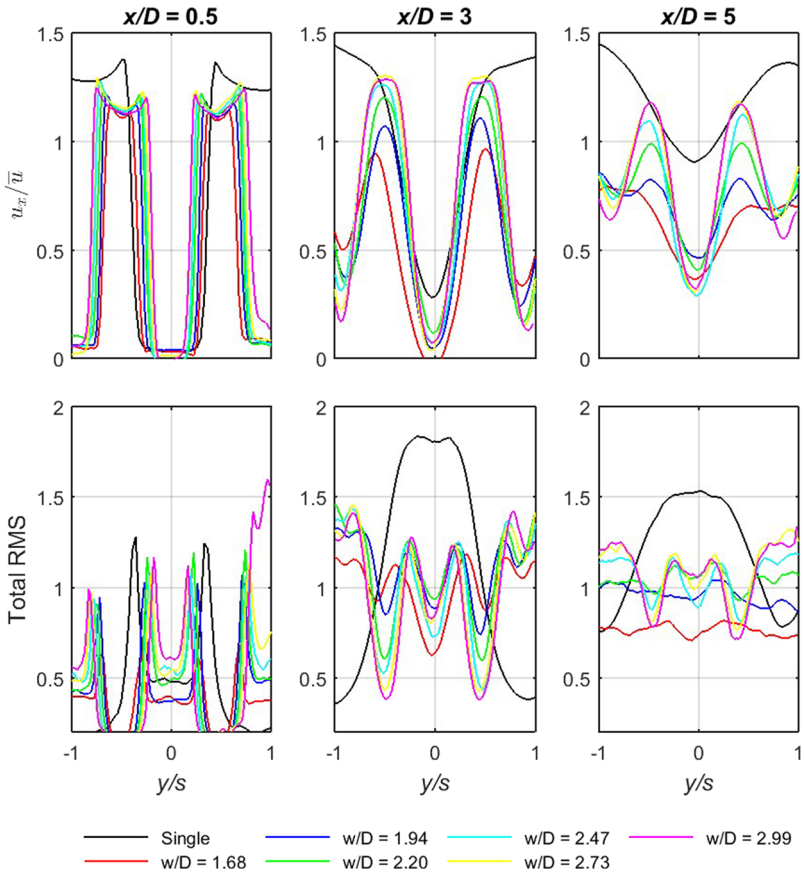

FIG. 4. Profiles of time-averaged axial velocity (top row) and total RMS fluctuations (bottom row) at three downstream distances.

case reveals three distinct regions of the flowfield as a function of downstream distance: a symmetric vortex shedding starting at approximately half a bluff body diameter downstream; a strong, asymmetric peak frequency starting approximately three bluff body diameters downstream; and a transitional period between the two regions. Figure 5 shows the peak Strouhal number, based on the bluff-body diameter, in each shear layer as a function of downstream distance, identifying the regions: shear layer shedding (I), transition (II), and wake shedding (III). These Strouhal numbers align well with the reported literature,[38,46] particularly in the wake shedding region, where the Strouhal number is $St_D = 0.28$. Whereas the vortex shedding frequency is constant downstream of $x/D = 2$, the regions upstream show significant variation in the frequency.

Proper orthogonal decomposition (POD) is used to understand the structure of these oscillations and the intermittency seen in the shear layer shedding region. Figure 6 shows POD modes 1 and 2 of both the axial and cross-stream velocity fluctuations. These first two modes for the single bluff-body flow can be identified as a mode pair based on their similar spatial patterns, energies, and frequency content. Because POD is an energy-based decomposition, the modes with the largest coherent fluctuations are identified first, thus the reason for these wake shedding modes to appear as modes 1 and 2. Combined, these two modes contain 42.5% of the fluctuating energy in the flowfield. These modes are highly identifiable as the von Kármán vortex street,[47] confirming the behavior of this flowfield with previous studies. The next several POD modes following the wake shedding modes are mostly related to the shear layer oscillations produced by the Kelvin-Helmholtz instability. Even higher-order modes have turbulent fluctuations scattered throughout the flowfield with no narrowband frequency content.

One of the focuses of this work is the investigation of "intermittency" in the flowfield. Here, we define intermittency not in a traditional turbulent sense,[48] but instead in the context

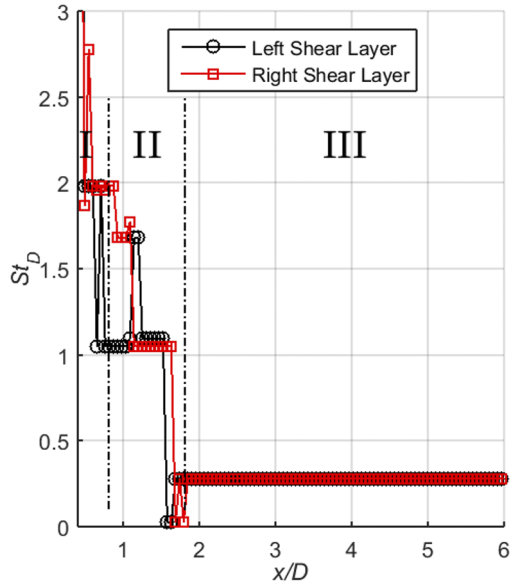

FIG. 5. Peak St_D as a function of downstream distance for the single bluff-body shear layers.

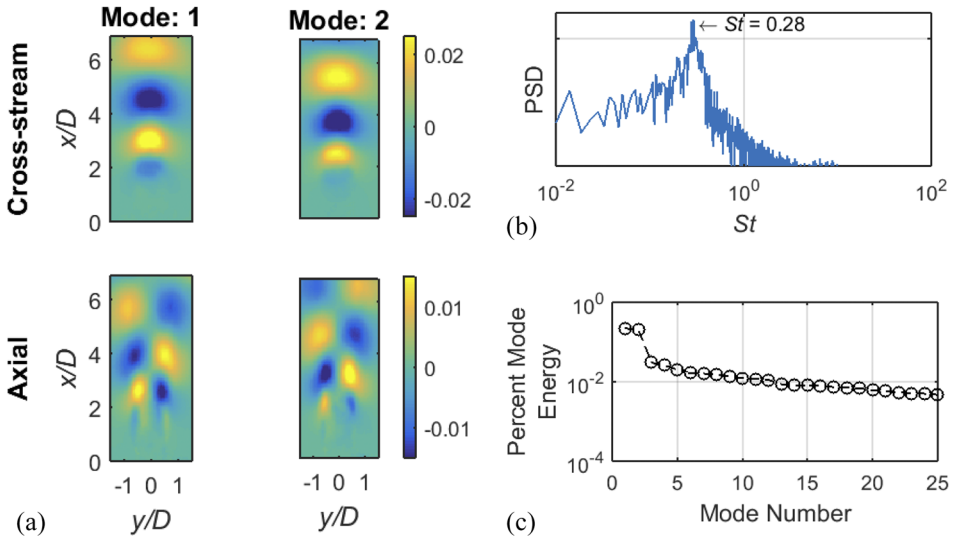

FIG. 6. POD results; modes 1 and 2 of transverse and axial (a) velocities, as well as the PSD of mode 1 (b) and energy distribution (c).

of the dynamics of the large-scale structures in the flowfield. In particular, we consider variations in vortex shedding frequency, phase, and strength to be signs of intermittency in the large-scale dynamics, as opposed to, for example, the prediction of a linear stability analysis or the behavior at a very low Reynolds number, which would result in just one vortex shedding frequency and consistent vortex strength over every cycle. For this single bluff body configuration, the existence of a transition region, as shown in Fig. 5, indicates jitter and intermittency in the flowfield, despite the consistency of the wake shedding downstream of this region. Wake vortices are formed at slightly different downstream locations in different cycles, a feature known as "phase jitter."[49] When multiple bluff bodies are placed in parallel, this leads to further intermittency and jitter caused by interactions between adjacent flows.

2. Dynamics of interacting flows

In the study of interacting flows, spacings of w/D = 1.68, 1.94, 2.20, 2.47, 2.73, and 2.99 are analyzed. Figure 7 shows a time series of instantaneous flowfields at w/D = 1.94 to illustrate an example of flow development in the interacting cases. The black triangles at the bottom of each flowfield show where the bluff bodies are located. A number of features are evident from these images. First, the wake shedding behind the bluff bodies is strong enough to be evident in the instantaneous flowfields; the oscillations in the streamlines indicate the trajectories of the coherent structures as they convect downstream and bend the flow around them. For example, wakes 1 and 3 begin the time series in phase, which is particularly evident by looking at the streamlines between x/D = 2-5 where vortex coherence is the highest. At the beginning of the time series, the oscillations from the right edge of wake 1 and the left edge of wake 3 are in phase, shifting left and right together. However, their phase shifts in images 4-6 until the wake oscillations are strongly out of phase in images 7-10.

Additionally, as the wakes behind the bluff bodies oscillate, they "squeeze" the jets between the bluff bodies and create pockets of high and low velocity that convect downstream

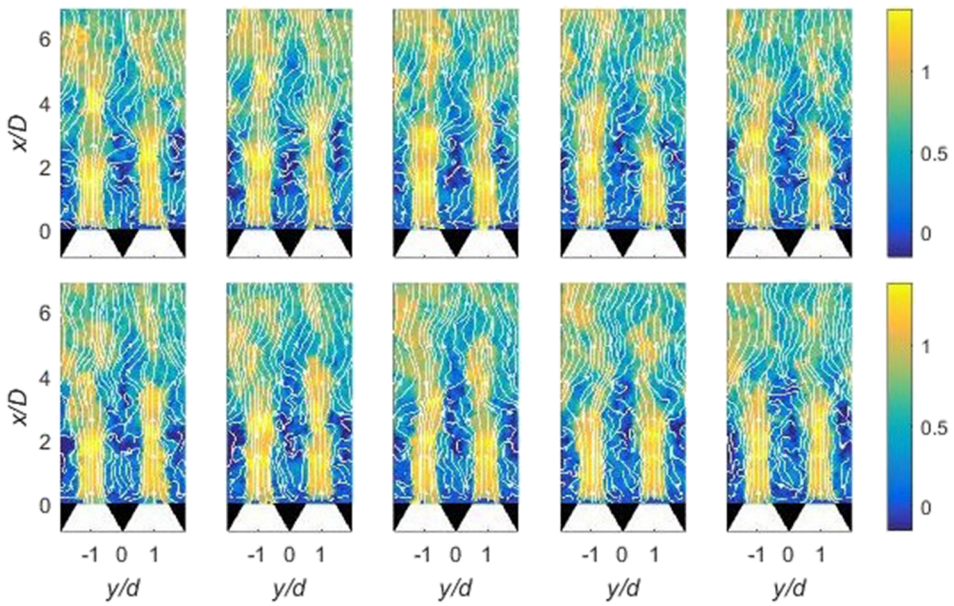

FIG. 7. Instantaneous velocity fields for w/D = 1.94, where colorbar is axial velocity normalized by the bulk velocity and snapshots (read left to right, top to bottom) are 5.3 ms apart.

with the coherent structures. An example of these pockets can be seen in the right jet in the bottom row of images. Here, a pocket of high velocity begins to form with a center near $x/D = 3$, where in the next image, the interaction of wake structures from wakes 2 and 3 creates a low-velocity disturbance near $x/D = 2.5$, downstream of the high-velocity pocket. The high-velocity pocket travels downstream, where the center is approximately located at $x/D = 3$, 3.5, 4, and 4.5 in the first four images in the bottom row; the pocket has largely broken up by the fifth image. These pockets seem to be formed when adjacent wakes oscillate out of phase such that both wakes bend in toward the same jet centerline together. The streamlines in the bottom row of images, and in the high-velocity pocket formed between wakes 1 and 2 in the first three images of the top row, show this out-of-phase bending.

The other observation from these instantaneous streamlines is the intermittent structure of the velocity deficit region behind each bluff body. The time-averaged flowfield in Fig. 2 shows that there is time-averaged recirculation at $w/D = 1.94$ but not as strong as that in the single-wake and $w/D = 1.68$ cases. The weak time-averaged recirculation is likely due to the highly intermittent behavior in the region downstream of each bluff body. While negative velocities are measured in each time instance in Fig. 7, the magnitude of the reverse velocity and its location varies significantly in time. Additionally, the apparent "sources" and "sinks" in the streamlines in this region are likely indicative of three-dimensional motion in this region that is not captured with the two-dimensional velocity measurement.

As identified in the single wake in Fig. 5, the interacting flows also exhibit three regions of coherent fluctuations in the flowfield. However, the phase jitter and intermittency increase significantly in the three-wake cases as compared to the single-wake case. Frequency spectra along the shear layers are calculated for all cases, and peak frequencies from three of the cases, $w/D = 1.68$, 1.94, and 2.73, are shown in Fig. 8 with identified regions in the same manner as the single bluff body. These three spacings are chosen as representatives of three regimes of interacting-flow behavior, which will be detailed in this section. In the shear layer shedding region (I), a distinct vortex shedding frequency of roughly $St_D = 1.57$ is present in all three cases. This frequency differs slightly from case to case, but not significantly. In the transition region (II), we see far more intermittency as compared to the single bluff body case. The interactions between shear layers from the interacting bluff bodies cause intermittency in the vortex development, resulting in vortex jitter, especially at smaller spacings. These variations in the vortex interactions cause more variation in the peak shedding frequency in this region. The wake shedding region (III) shows a dependence of vortex shedding frequency on spacing; the wake shedding frequency found at $w/D \geq 1.94$ is a very similar frequency as that of the single bluff body in that region ($St_D = 0.28$). In this range of $w/D \geq 1.94$, region III begins farther downstream as the spacing increases.

Previous studies suggest a strong level of interaction between the wakes at intermediary spacing levels, as in the work of Alam *et al.*[23] In these cases, the dominant shedding mode is still the BVK vortex shedding at a similar frequency to that of the single bluff body, but there is intermittency in the relative phase of the vortex shedding from one wake to another; we quantify this intermittency in Sec. III B 3. Despite the intermittency in phase, the frequency is relatively constant, which is reflected in Fig. 8(b). At the farthest spacings, as in Fig. 8(c), the wake interaction is relatively weak as the mutual induction between vorticity in adjacent shear layers is weaker. These wakes still display BVK wake shedding, although the vortex inception point is further downstream as a result of the change in the time-averaged flow structure (Fig. 2) relative to the single wake. For spacings of $w/D < 1.94$, the primary peak Strouhal number is different from the single bluff body case, meaning that the level of interaction between adjacent flowfields is significant enough to change the instability characteristics, and hence vortex shedding frequencies and structure, in the combined flowfield. Recent work by Sebastian *et al.*[50] has indicated that spacing can significantly impact the stability characteristics of multi-wake systems.

Because POD is an energy-based decomposition and wake fluctuations contribute to the highest energy velocity

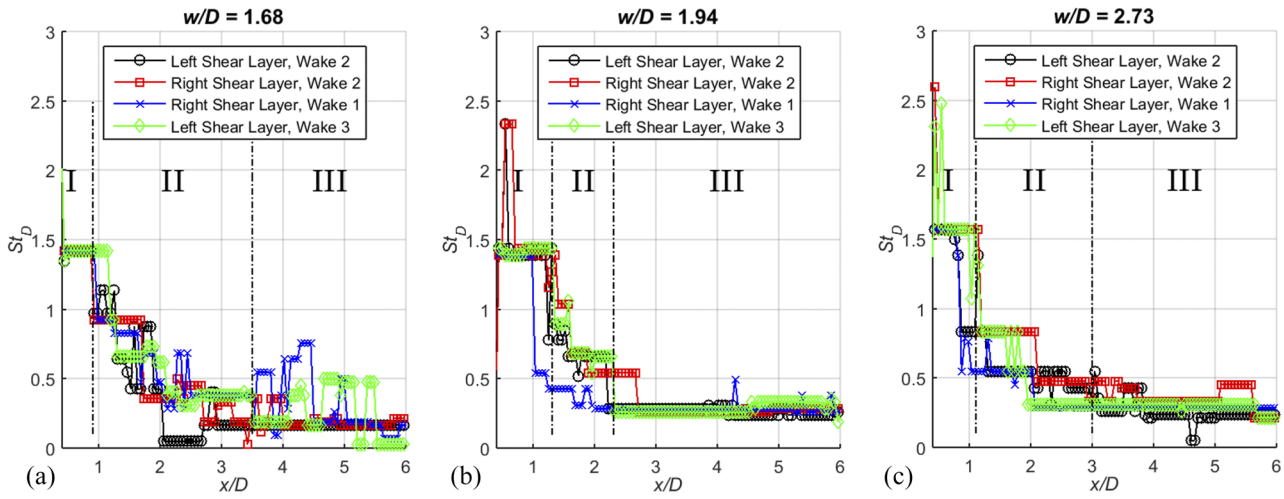

FIG. 8. Peak frequencies along shear layers in the multiple bluff body cases of $w/D = 1.68$ (a), 1.94 (b), and 2.73 (c) with identified shear layer shedding (I), transition (II), and wake shedding (III).

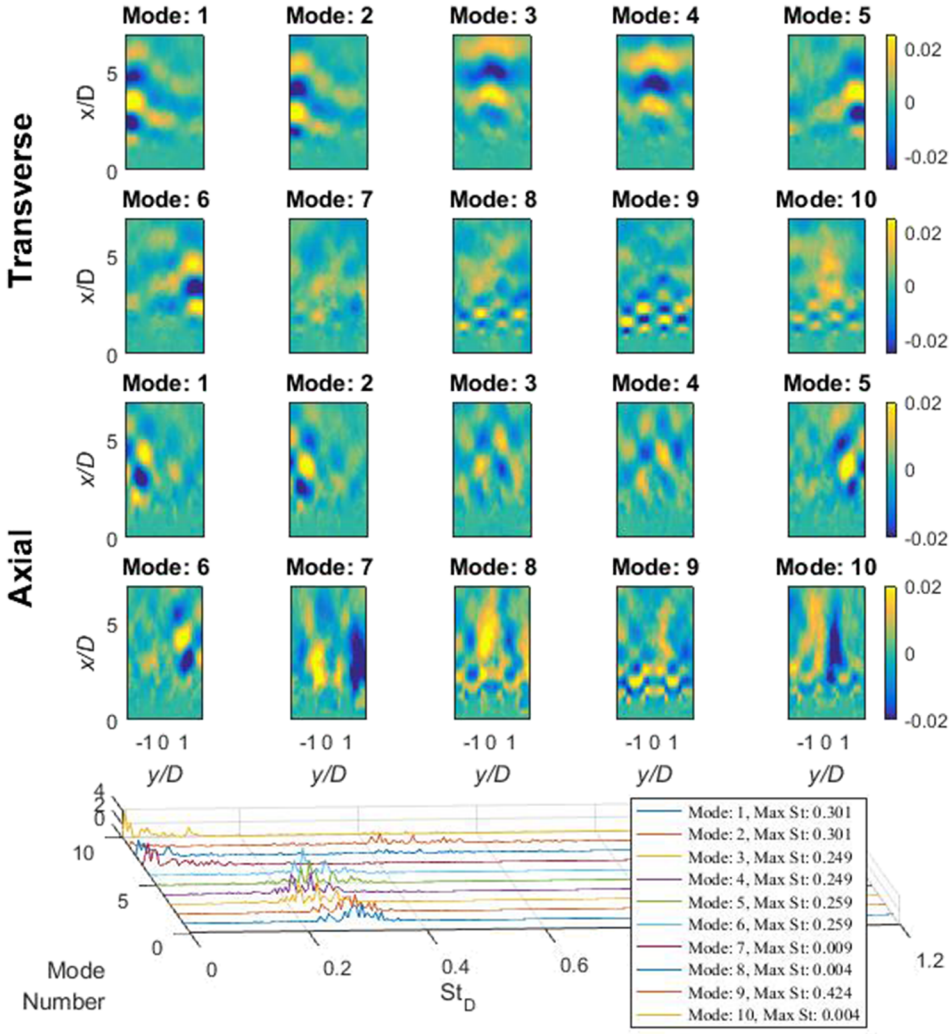

FIG. 9. Information on modes 1-10 for w/D = 1.94. The transverse spatial modes are on the top two rows, and the axial spatial modes are on the two rows below those.

fluctuations, the first 6 or 7 modes of the POD in all cases consequently contain fluctuations that are strongly related to the coherent structures in the downstream wake region of wake 1, wake 2, and wake 3. A typical decomposition of these wake shedding modes can be seen in Fig. 9, where details of modes 1-10 for w/D = 1.94 are shown as an example. Mode pairs can be identified similarly to the first two POD modes of the single wake case; these include modes 1 and 2, modes 3 and 4, and modes 5 and 6. Modes 1 and 2 show wake shedding of wake 1, on the left-hand side of the flowfield, and the shift of one mode relative to the other is indicative of convection in the downstream direction. Similarly, modes 3 and 4 are indicative of vortex shedding in wake 2 (in the center), and modes 5 and 6 are indicative of vortex shedding in wake 3 (right-hand side). The decomposition of the motion from each of the three wakes into separate modes should not be interpreted too literally; the eigenvalue decomposition does not inherently recognize that these structures originate from three separate bluff bodies. Instead, it is important to note that these six modes have the highest mode energies, similar structure, and similar frequency content.

The frequency spectra of modes 1-6, where the spatial modes strongly correspond to wake shedding, are similar to one another. Their maximum values are also close to the peak Strouhal number in the first two modes of the single bluff body case, St_D = 0.28, but are not as narrowband as in the single-wake case. Mode 7 shows little coherence in either wake shedding or shear layer shedding regions and thus very little narrowband content in temporal mode spectrum. Modes 8-10 mostly indicate shear layer shedding, based on the spatial modes, and the temporal spectra show meaningful local maximums near St_D = 0.4-0.5. This type of pattern where wake modes transition to shear layer modes is typical among all the cases; POD modes of the other spacings are provided in the supplementary material.

3. Interacting wake phase dynamics

The previous analysis shows that the downstream wake behavior in both the single- and multiple-wake cases dominates the fluctuating energy of the flowfield and hence represents the most critical dynamics in the flowfield. In particular, we are interested in the relative phase between vortex shedding in the wakes of the three bluff bodies, which could not be gleaned from the POD analysis. Previous studies of dual-wake systems showed that the relative phases between wake shedding could vary with spacing.[10,23] Additionally, studies that described these dynamics disagreed about their behavior, as authors described the dynamics as either random[16] or deterministic.[19,20] The intermittency seen in the three-wake

flowfield indicates a switching between coherent and incoherent motions, which is suggestive of a random process rather than a deterministic one. In this section, we describe the methods for calculating the phase relationships between motions in different wakes, analyzing one case as an example of the intermittent phase-switching behavior. We then propose a statistical description of these dynamics as a means to quantify the behavior of multiple-wake systems.

To clarify the wake behavior further, POD modes were reconstructed into a time series of velocity fluctuations. Modes for this reconstruction were selected based on their spatial structure, frequency content, and energy, as discussed in reference to Fig. 9. Modes that contained wake-related motions (significant oscillations downstream of $x/D = 3$) were used in the reconstruction. This process required some level of user input, and more information about the POD modes is provided in the supplementary material. The sensitivity of the results to the inclusion of more modes is minimal, particularly because higher-order modes mostly contain shear layer oscillations rather than wake oscillations, adding low-energy noise to the analysis of wake dynamics. Table III shows the number of POD modes used in each of the reconstructions at each operating condition.

To better quantify the dynamics of the wake, we extract velocity signals from three "probes" in the downstream regions of wakes 1, 2, and 3. These probes consist of the median of the data from windows of 3×3 interrogation windows in the flowfield. This creates a one-dimensional, real-valued signal of reconstructed cross-stream velocity fluctuations. The locations of these probes were different for each bluff body spacing, as the structure of the flow changed significantly with bluff-body spacing. To calculate the probe location, the RMS of the reconstructed transverse velocity signal was summed along the transverse direction at each downstream location; these profiles are shown in Fig. 10. The location of the maximum value of the summed RMS was chosen as the downstream location of the probes. The non-dimensional cross-stream locations were held constant through the cases at $y/D = -\frac{7}{8}(w/D)$, 0, and $\frac{7}{8}(w/D)$ because the outer wakes tend to deflect toward the center of the experiment and these cross-stream, non-dimensional coordinates account for that deflection. The sensitivity of the following results was shown to be minimal when varying the probe location by distances of approximately $0.2D$ in all the directions. Although this is only a small portion of the flowfield, any further probe displacement would extend out of the region of interest and distort the results.

A Hilbert transform is performed on each probe signal to determine the instantaneous amplitude and phase of the oscillations in each wake. The Hilbert transform requires a strongly periodic signal; thus, the POD reconstruction is critical to extract useful phase information. As an example of this process, Fig. 11 shows the entire time signal of each of the probe locations for $w/D = 1.94$. Three portions of the time series are highlighted to show particularly interesting phase behavior; the first time series, from $t = 0.195$ to 0.243 s, is the same data that were shown in the instantaneous velocity fields in Fig. 7. These three behaviors are not necessarily an exhaustive list of the types of behaviors found in the signal but instead are used to show the types of information that can be learned from this probe phase analysis. This example is also used to show how the oscillations in the probe signal are representative of large-scale dynamics in the flowfield, as the reconstructed velocity fields from the POD are provided for critical times in the time series. The three behaviors discussed are a switching process; steady-state, in-phase behavior; and steady-state phase behavior that is neither in-phase nor out-of-phase. Snapshots of the reconstructed cross-stream velocity fluctuations are shown below at the time instance of the black, dashed line.

TABLE III. Number of POD modes used in the reconstruction of wake behavior.

w/D	1.68	1.94	2.20	2.47	2.73	2.99
POD modes	1-7	1-7	1-6	1-7	1-6	1-8

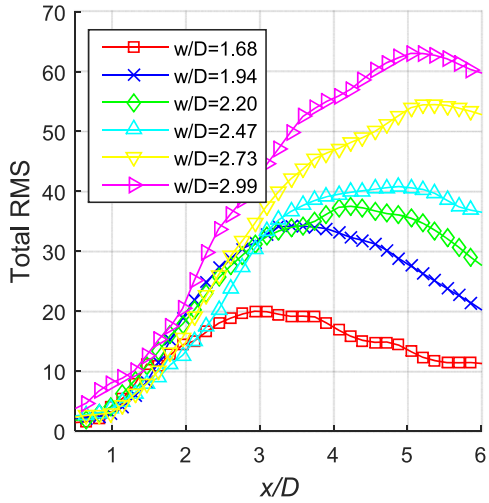

FIG. 10. Summed RMS from POD reconstruction as a function of downstream distance.

The first time segment shows a switching process from in-phase behavior between wake 1 and wake 3 [Fig. 11(a)] to out-of-phase behavior of wake 1 and wake 3 [Fig. 11(b)]. In-phase behavior of wake 1 and wake 3 lasts approximately 0.085 s, or 4 cycles, and then a transition period occurs where the phase between wakes 1 and 3 gradually increases over approximately two cycles until they are out-of-phase. During this first period (before $t = 0.195$ s) when wake 1 and wake 3 are in phase, the fluctuations of wake 2 are small, but during the transition period, the fluctuations become larger. After the transition period, the fluctuations of wake 2 are of the same magnitude of wake 1, and wake 2 oscillations are also in-phase with those in wake 1. This phase switching in wakes 1 and 3 is quite clear in the reconstructed velocity fields, where at $t = 0.195$ s, the probes in wakes 1 and 3 are located in the middle of coherent structures of positive velocity fluctuation, whereas at $t = 0.243$ s, the probe in wake 1 is located in the middle of a coherent negative velocity fluctuation. This comparison shows that the probes are placed in the right location to capture the fluctuations of each wake.

The second behavior, the in-phase behavior between wake 1 and wake 3, is shown in Figs. 11(c) and 11(d). Here, wakes

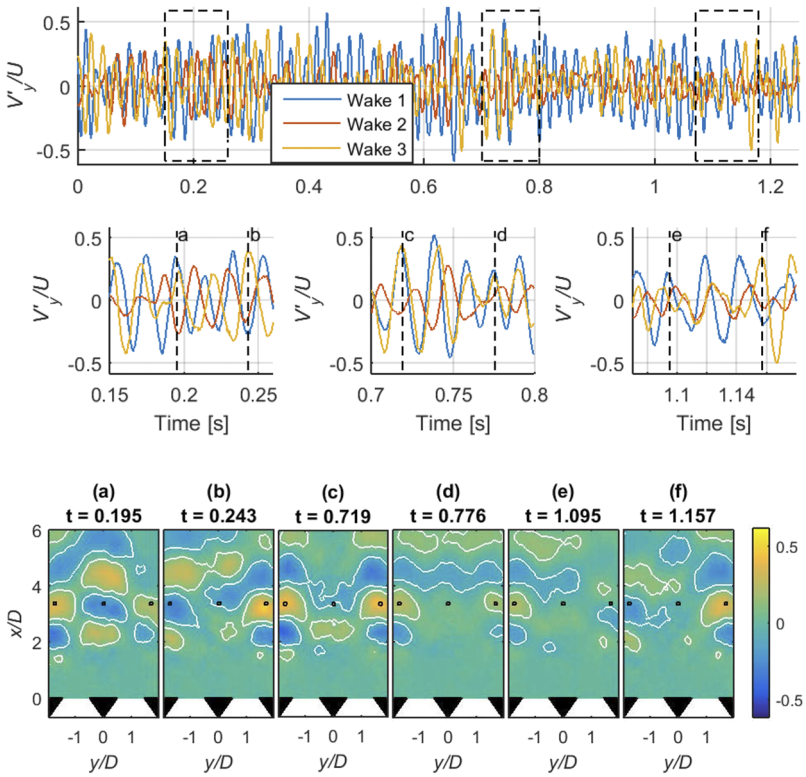

FIG. 11. Cross-stream velocity signal of the three probes in the wake region with three highlighted regions and instantaneous snapshots of the flowfield (contours at $V_y/U = 0.1$ and -0.1). Probe locations are indicated in the flowfield.

1 and 3 are in-phase for a relatively long duration, and wake 2 behavior varies during this time. In this particular case, wake 2 is typically acting out-of-phase relative to the other two wakes, but the magnitude of the velocity fluctuations in wake 2 varies greatly during this time. There is also an instance at $t = 0.776$ s where wake 2 "skips" a cycle and then resumes its normal out-of-phase cyclic pattern. The fluctuation amplitudes of wakes 1 and 3 are much larger than that of wake 2 during this time period. This amplitude difference is reflected in the RMS values in Fig. 3, where the RMS velocity of wake 2 is relatively small as compared to that of wakes 1 and 3. The in-phase oscillations in wakes 1 and 3 are also evident in the reconstructed velocity fields, where at both $t = 0.719$ and $t = 0.776$ s, the probes are located in regions of coherent positive velocity fluctuation. The intermittency of wake 2 is also evident by the less coherent structures present in the center of the flowfield.

The third behavior is one where the wakes show intermittent, and non-repeatable, phase behavior, as shown in Figs. 11(e) and 11(f). For the entire duration shown, wake 2 is slightly trailing wake 1 by a phase that is neither in-phase nor out-of-phase but is constant. The magnitude of the fluctuations for wake 2 is significantly smaller than those in wakes 1 and 3, as previously noted in Fig. 3 for the RMS of the velocity signal. Wake 3 repeatedly "skips" phases in the cycle, allowing the phase between wake 3 and the other two wakes to drift over this time period, as the phases of wake 1 and 2 stay constant. Not only does the phase of wake 3 drift during this time period, but also the amplitude, where changes in the fluctuation strength of wake 3 are seen during these periods of random phase activity. These three example behaviors are meant to show significant variations in the wake shedding phase that occur over time, as well as the ability of the probe signal to faithfully capture the flowfield dynamics.

To quantify the phase between vortex shedding in each wake throughout the time series, phases are analyzed in a statistical manner. The phase of the signal, θ, of each wake is found by calculating the angle (from $-\pi$ to π) from the Hilbert transform. Relative phases, ϕ, are then calculated between the oscillations in each wake. For example, the phase between wake 1 and wake 2 is $\phi_{21} = \theta_2 - \theta_1$. The relative phases calculated using this method can range from -2π to 2π. Because the phase angle is 2π-periodic such that phase angles with a difference of 2π are equivalent, the phase angle is "wrapped" so that relative phases are in the range of $-\pi$ to π. Figure 12 shows the probability of these relative phases with 24 linearly spaced bins for several cases.

Twenty-four evenly spaced bins were used, resulting in bin widths of $\pi/12$ from $-\pi$ to π. The number of occurrences in each bin was normalized by the number of total samples to find the probability. The first case of $w/D = 1.68$ highlights a few key features found among the different cases. Most notably, some of the relative phases tend to be centered about a specific phase. For this case in particular, ϕ_{32} is centered about $\pi/6$. ϕ_{31} shows that the probability of the phase is highest near $-\pi$ and π. Because phase is 2π-circular, ϕ is "wrapped" to the range of 0–2π, and the center would be approximately π, meaning the right and left wakes are typically out-of-phase with one another. ϕ_{21} appears to be very weakly centered at a relative phase of $-2\pi/3$, where the relative phase is wrapped similar to ϕ_{31}.

For $w/D = 1.94$, not all of the phases are centered about a particular phase. Instead, both ϕ_{31} and ϕ_{32} are evenly distributed. This would indicate that for these cases, there is no favored relative phase and the wakes are equally likely to oscillate with a random relative phase. However, for ϕ_{21}, a defined preference can be found at approximately $-3\pi/4$, which shows that the wakes favor a phase that is neither entirely in-phase

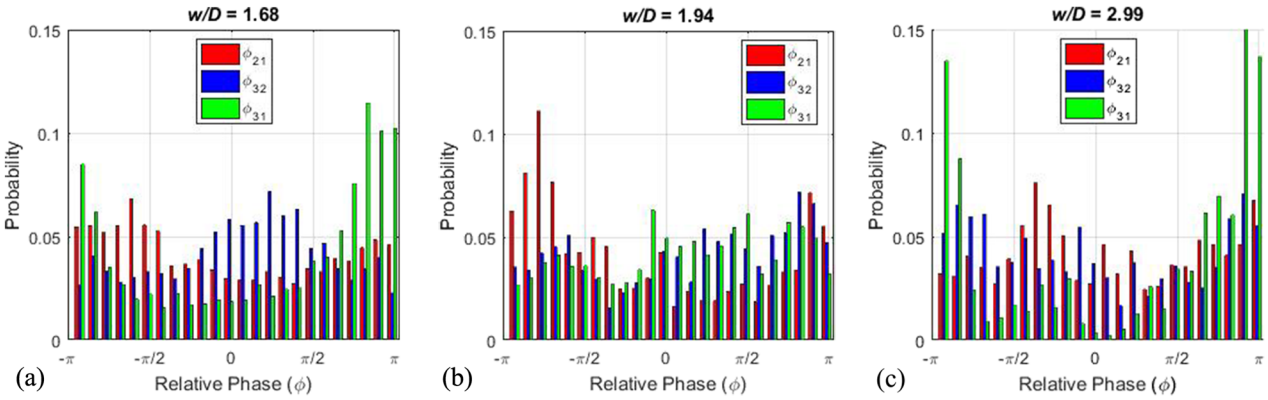

FIG. 12. Relative phase from the Hilbert transformation for w/D = 1.68, 1.94, 2.99.

nor out-of-phase. For w/D = 2.99, the most probable state for ϕ_{31} is close to out-of-phase and the other two relative phases do not have any shape, similar to w/D = 1.94, ϕ_{31}, and ϕ_{32}. One key difference in the distribution of ϕ_{31} for w/D = 2.99 and ϕ_{21} for w/D = 1.94 is the spread of the data at the approximate center value. The latter has a much smaller spread than the former, as evidenced by how gradually the bins surrounding the approximate center decrease as the difference between the relative phase bin and the center increases.

To quantify the characteristics of these phase probabilities, a Gaussian distribution of the form $a\exp[-((\phi-b)/c)^2]+d$ is fitted to the binned data for all cases, where a, b, c, and d are free variables and ϕ is the binned relative phase. The fit uses a robust bi-square fitting technique, which iterates to find a solution based on user-input initial guesses. The resulting fit values are shown in Table IV; cases where relative phase probabilities were relatively uniform are marked as "uniform," and no Gaussian fit is applied.

Each of these free variables and coefficient of determination (R^2) values provides critical information about the behavior of these wake systems. The coefficient of determination quantifies how well the Gaussian distributions fit the corresponding binned data, where a value of 1 means the approximated distribution fits the data perfectly and 0 does not. The value d represents the value that the fitted curve asymptotically approaches outward from the center. The value a is the height above d at the approximated maximum of the fitted curve and can be physically interpreted as the frequency of the most probable phase. As a increases, the system spends more time in a single, most probable mode. The value b is the center of the fitted curve, where the maximum is located, and can physically be interpreted as the most probable phase shift. The value c describes the spread of the distribution or twice the variance. All of these variables are important to consider when interpreting how well the normal distribution fits the data. Some of the data did not fit well to a normal distribution, based

TABLE IV. Gaussian fit information for relative phase probabilities.

Spacing (w/D)	Relative phase (ϕ)	Shifted	a	b	c	d	R^2
	2-1	Yes	0.027	3.823	1.608	0.029	0.883
1.68	3-2	No	0.035	0.552	1.141	0.030	0.818
	3-1	Yes	0.085	2.780	0.864	0.020	0.979
	2-1	Yes	0.053	3.685	1.127	0.023	0.811
1.94	3-2			Uniform			
	3-1			Uniform			
	2-1			Uniform			
2.20	3-2			Uniform			
	3-1	No	0.055	0.002	0.384	0.024	0.710
	2-1	Yes	0.041	2.097	1.421	0.016	0.836
2.47	3-2	Yes	0.029	3.228	0.896	0.026	0.652
	3-1			Uniform			
	2-1			Uniform			
2.73	3-2			Uniform			
	3-1			Uniform			
	2-1			Uniform			
2.99	3-2	Yes	0.030	3.361	0.929	0.034	0.576
	3-1	Yes	0.120	2.892	0.728	0.016	0.929

on quantified metrics in Table IV, and were marked as "uniform," which is the distribution that more closely resembled the data.

One of the most notable results from this analysis is the behavior of ϕ_{31}. At the smallest spacing and the largest spacing, there is a strong, out-of-phase relationship between the wakes (see Fig. 11 for visualization of out-of-phase relationship in the flowfield) based on the large coefficient of determination and high a values. The Gaussian shape and significant center peak can also be seen in the histograms. However, these out-of-phase behaviors at both small and large spacings may be the result of different vortex shedding processes because the frequency spectra along the shear layers (Fig. 8) indicate that the peak Strouhal number in the wake region is different for these cases. Also, the prominence of a peak in the histograms for ϕ_{21} and ϕ_{32} also varies with small and large spacings. At the smallest spacing, the Gaussian shape is still present, despite being weaker than that of ϕ_{31}. At the two largest spacings, ϕ_{21} and ϕ_{32} do not have a distinct Gaussian shape as compared to the smallest spacing but have out-of-phase ϕ_{31}. These findings suggest that at small w/D values, the outer wakes behave predominately out-of-phase, and as the spacing is increased, this relative wake behavior is first more intermittent and then transitions back to out-of-phase behavior at larger spacings.

For the three cases where ϕ_{31} is not strongly out-of-phase, w/D = 1.94, 2.20, and 2.47, there are still distinct behaviors in some of the relationships between either set of adjacent wakes. Particularly for w/D = 1.94 and 2.47, ϕ_{21} has a strong Gaussian fit where the phase is centered near $5\pi/4$ and $2\pi/3$, respectively. This result indicates that wake 1 tends to trail wake 2 by about $\pi/4$ for w/D = 1.94, but for w/D = 2.47, wake 1 leads wake 2. Part of the time signal shown in Fig. 11(c) highlights an instance of this phase relationship in the signal for w/D = 1.94. For w/D = 2.20, very weak in-phase behavior is noted for ϕ_{31}. These results indicate that at intermediate spacings, where w/D = 1.94-2.47, the wakes must be interacting to some degree because some of the phase relationships are mildly centered about a particular phase, but wake behavior is largely stochastic as most of the distributions are uniform.

In addition to the phase statistics, we quantify the statistics of the duration that the system spends at a given phase using exponential distributions. Durations are calculated for all cases with eight phase centers, with a bin width of $\pi/2$, ranging from $-3\pi/4$ to π, where for the bin of π, $-\pi$ to $-3\pi/4$ was used for the upper range because phase is 2π-circular. The length of time that the relative phases stay in a particular phase is determined by the number of consecutive data points that stay within the bin width. The time was normalized by the dominate frequency seen in the wake region, which was 48 Hz for all cases except w/D = 1.68, which had a dominant frequency of 32 Hz, to obtain number of cycles that the system retains a certain phase. A short median filter is used to ensure extraneous data points do not truncate the number of consecutive data points during a well-behaved phase pattern. Binned data of the phase durations with fitted exponential curves overlaid are shown for four key cases in Fig. 13; the assumption of an exponential distribution follows that of Kim and Durbin,[16] although the data in the current study contain significantly fewer bins than the analysis by these authors. These cases were chosen as they represent the four important cases from the normal distributions in Table IV: small spacing (w/D = 1.68), ϕ_{31} out-of-phase; intermediate spacing (w/D = 1.94), ϕ_{32} uniform distribution; intermediate spacing (w/D = 2.47), slightly out-of-phase normally distributed; and large spacing (w/D = 2.99), ϕ_{31} out-of-phase.

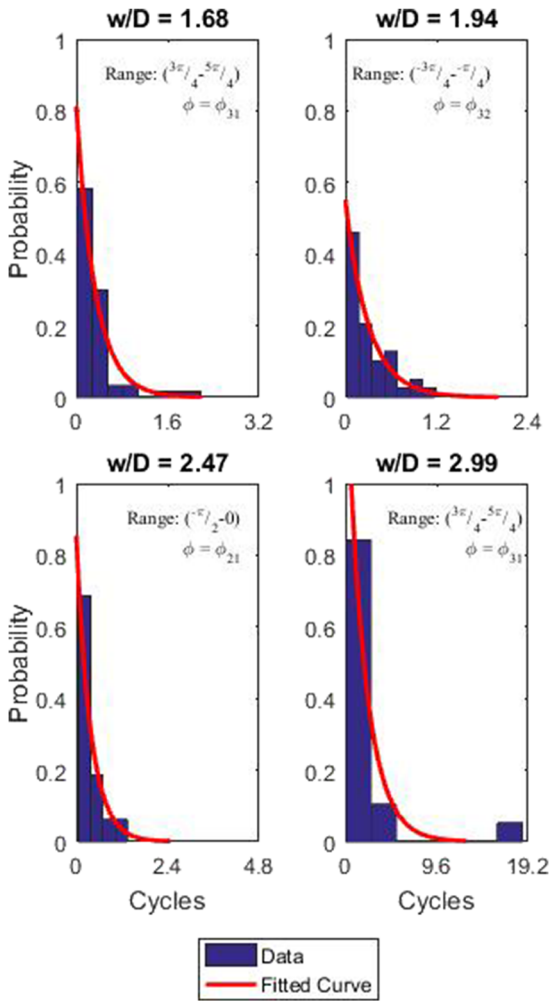

FIG. 13. Binned durations with fitted curve overlaid for cases and range listed earlier.

For all of the cases, the most probable duration of time that a relative phase stays close to a particular phase is the bin with the shortest duration. The second shortest bin has the next highest probability, and the probability continues to decay as the bin time increases. For these reasons, all these phase durations fit well to an exponential curve, despite having significantly different relative phase dynamics, as in Fig. 12. This exponential curve indicates that the changes in phase are mostly random rather than a deterministic or cyclic process; otherwise, we would expect a different type of distribution to fit the phase duration data, such as a Gaussian distribution. These results mirror investigations in dual wake systems that found the "flip-flopping" process also fit an exponential curve.[16] Although these are physically different processes, the behavior of the arrival times is similarly stochastic.

IV. DISCUSSION

In this work, we have considered the dynamics of three-wake systems and used statistical analysis to quantify the wake vortex behavior. We consider three-wake systems at moderate Reynolds numbers, where three-wake systems have only been investigated by a few authors.[11,22,27] The majority of these studies were at low Reynolds numbers (Re $\sim O(100)$) where shear layer dynamics play a relatively unimportant role, whereas our results identify the shear layer as a key source of intermittency in the flowfield.

One key finding from this work is that three-wake systems behave similar to two-wake systems in a number of ways. First, the dynamics of the three-wake system are highly dependent on bluff-body spacing, and the regimes of behavior for small, intermediary, and large spacings align well with the behavior of two-wake systems. In particular, the dynamics of flows at small and large spacings are more deterministic than those at intermediary spacings. We have quantified this using Gaussian distributions of phase relationships between vortex shedding events in each wake and have investigated the structure of these flows using POD. The results have indicated that high levels of interaction at small spacings may result in "lock-on" of vortex shedding throughout the system. The structural sensitivity analysis of Carini *et al.*,[21] though at a much lower Reynolds number, indicates that interaction between shear layers at the bluff-body separation point may result in coherent interaction between adjacent flowfields. The reasons for coherent, synchronized behavior at large spacings with small levels of interaction are less clear. For each wake individually, the structure of the wake approaches that of a single wake as the spacing between bluff-bodies increases; the similarity of the vortex shedding Strouhal numbers between the large-spacing cases and the single-wake case also indicates this similarity. However, the statistical analysis of the wake-to-wake phase relationships also indicates more regular phase behavior for large spacings, which is likely driven by different physics than the shear layer interaction that dominates the small-spacing cases. The intermediary regime, with its high levels of vortex shedding intermittency and uniformly distributed phase relationships between wake vortex shedding events, mirrors the intermediary regimes of the two-wake systems seen by many in the two-wake literature.[12,23,28] The mechanism by which this regime displays more random behavior, though, has not been proposed and is not apparent from the present data or past literature.

A second key result is the use of statistical descriptions for flowfield dynamics in multi-wake systems. While a mechanistic understanding of behavior of the flow, like those proposed by Wang and Zhou,[18] is important, these physics are based on individual events. To consider larger issues such as drag and system control, a statistical approach provides critical information about the state of the system over a period of time, as well as the most likely behavior of a given system. The statistical analysis presented here provides quantifiable evidence for the categorization of system behaviors as a function of spacing and helps more concretely define the "close," "intermediary," and "large" spacing regimes. These statistical descriptions, linked with reduced-order analysis like POD, may be more important when considering even higher Reynolds number flows, where turbulent fluctuations may make it difficult to observe these regimes from high-speed imaging, as was done in many two-wake studies. Additionally, the statistical description of the flowfield provides quantification of the intermittency present in the flowfield. While many metrics have been developed for quantifying intermittency, including recurrence quantification analysis from recurrence plots[51] and wavelet analysis,[52] a statistical description, particularly when fit to a known distribution, provides powerful quantification of system dynamics.

A final key result is the impact that boundary conditions may have on the structure and dynamics of the flowfield. This study was conducted in an experiment where quiescent, ambient air is entrained on either side of the three-wake system. Many of the previous studies in two- and three-wake systems used wind tunnels or water tunnels, with a mean-flow boundary condition on the outside of the wake system and, much further away, a hard wall. The entrainment that our ambient condition drives may change the structure and dynamics of the system relative to the tunnel configurations. In particular, we have identified that the entrainment changes the structure of the time-averaged flowfield downstream of the bluff bodies, where the flow converges toward the centerline; this is a common phenomenon in multiple-jet studies, which typically also have ambient boundary conditions. Additionally, the shear generated between the flowfield and the quiescent ambient is an additional source of turbulence that is not present in a tunnel configuration, which may alter the RMS velocity and vortex dynamics, particularly of the outer two wakes.

A final consideration of this study is the underlying assumption we have made as to the structure of the flowfield. Here, we have treated the flowfield as an ensemble of three wakes, where these individual unit flows interact and the dynamics of the ensemble differ from that of the unit flow as a result of flow interaction. We predicated our analysis on this structure largely because this was the context that the previous literature provided. The studies of dual-wake and dual-jet systems considered the interaction of adjacent unit flows, which can be changed by varying the spacing in between the flows. As our results were congruent with what had been observed in the dual-wake literature, we discussed our results in this "ensemble" context. An equally valid approach to addressing a flow of this complexity is not to see it as the superposition of three unit flows, but rather a single flowfield, where the characteristics of this single flowfield vary as the boundary conditions of the flowfield (here, the bluff-body spacing) change. This approach is more congruent with the idea of flow stability, where the flow response to an ansatz of perturbations describes the dynamics, following that of Carini and co-workers.[19–21] We hope, in future, to explore this second view of the interacting flow problem to gain further insights into the dynamics of the flow and the origin of intermittency in the large-scale dynamics.

V. CONCLUSIONS

This study experimentally investigates the impact of spacing of three triangular bluff bodies on the flowfield structure and dynamics. Interaction between adjacent wakes results in

bias in the time-averaged flowfield. Because ambient air is the boundary condition, the four "jets" around the bluff bodies merge as the flow moves downstream for all cases. RMS velocities, particularly in the shear layers, are found to be larger for the outer wakes and may contribute to this merging. The single wake dynamics compare well with previously reported data, including similar POD characteristics in the first two modes and downstream vortex shedding behavior, where a peak Strouhal number of $St_D = 0.28$ emerges. The three-wake systems have noticeably different flow dynamics than the single wake case. Plots of the Strouhal number as a function of downstream distance reveal a change in the structure and dynamics of the flowfield as a function of spacing, creating three behavioral regimes at small, intermediary, and large spacings. At the smallest spacing $w/D = 1.68$, the peak Strouhal number in the wake region is unlike every other case. Both the intermediary and large spacings have a peak Strouhal number close in value to that of the single bluff body, but vortex shedding at the intermediary spacings is much more intermittent than at small and large spacings.

To further investigate wake behavior, proper orthogonal decomposition is performed on the flowfields with multiple bluff bodies. The resultant modes of the multiple bluff body cases show primarily wake fluctuations for the first 6-8 modes, determined by studying where the largest fluctuations are from the spatial modes, the temporal mode shapes, and the amount of energy in the mode. The modes most closely contributing to the wake behavior are reconstructed into a time-series. Three probes extract this reconstructed velocity signal at a location where the RMS summed along the transverse direction is greatest. A Hilbert transform is performed on each of these signals to acquire instantaneous phase of each analytic signal. The instantaneous phase is compared among different wake pairs.

Histograms of relative phases are presented for three different multiple bluff body cases. The patterns exhibit primarily out-of-phase vortex shedding of wake 1 and wake 3 for cases $w/D = 1.68$ and 2.73. But the underlying mechanism may be different because the Strouhal numbers in the wake region are significantly different. For $w/D = 1.94$, no pattern exists for relative phase between wake 1 and wake 2, but there is for the relative phase between wake 1 and wake 2. Normal distributions were fitted to the data. This statistical analysis helps quantify how wakes interact with one another and suggests that the intermittent behavior seen at intermediate spacings interferes greatly with regular wake behavior, unlike that seen in the small and large spacings. From this, the relative phases of adjacent wakes sometimes display a phase relationship centered about a particular value not indicative of in-phase or out-of-phase behavior. Otherwise, the dominate feature is the out-of-phase behavior of the outer wakes.

SUPPLEMENTARY MATERIAL

See supplementary material for additional POD decompositions at all three-wake spacings, as well as the Gaussian fits for each of the phase-angle distributions.

ACKNOWLEDGMENTS

This work was partially supported by the Air Force Office of Scientific Research under contract monitor Dr. Chiping Li, Award No. FA9550-16-1-0075. The authors would like to thank Wyatt Culler for his support with the Hilbert transform analysis.

APPENDIX: VELOCITY UNCERTAINTY

Uncertainty measurements were calculated in Davis using the correlation statistics method proposed by Wieneke.[53] Figure 14 shows the normalized mean velocity uncertainty and normalized RMS velocity uncertainty along the transverse direction at the center of the probe locations. The legend

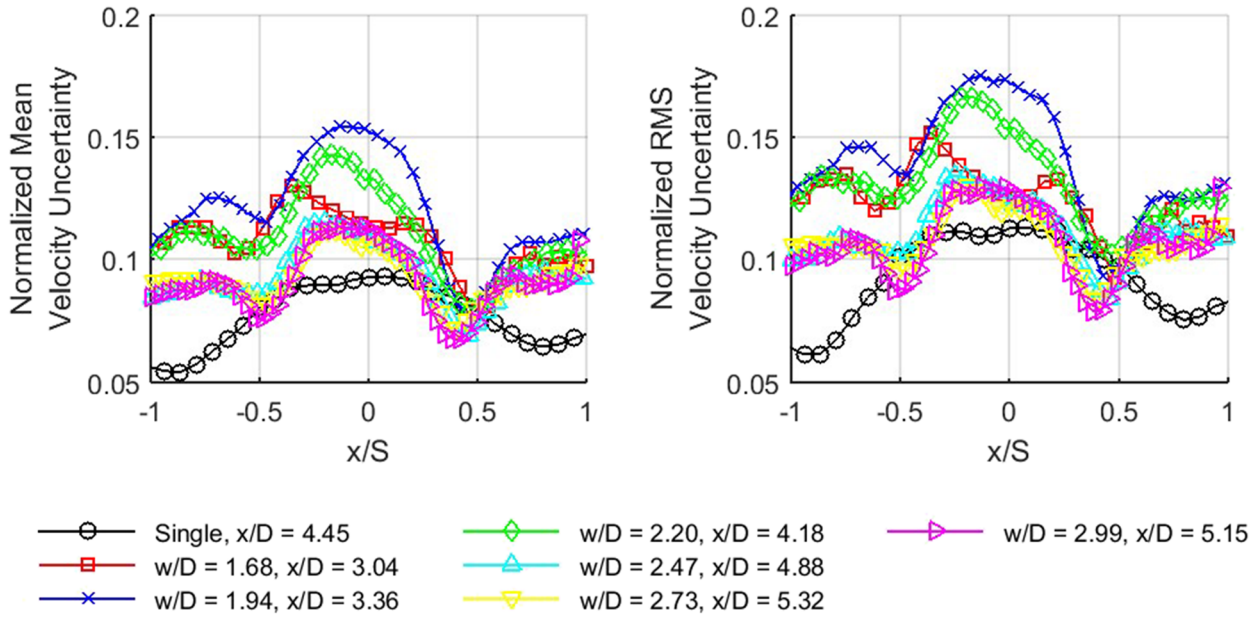

FIG. 14. Uncertainty levels in the time-averaged (left) and RMS (right) velocities.

identifies the case and x/D location, as the probe location varies with spacing.

[1]A. Nasr and J. Lai, "Two parallel plane jets: Mean flow and effects of acoustic excitation," Exp. Fluids **22**(3), 251–260 (1997).
[2]S. Yuu, F. Shimoda, and T. Jotaki, "Hot wire measurement in the interacting two-plane parallel jets," AIChE J. **25**(4), 676–685 (1979).
[3]N. Ko and K. Lau, "Flow structures in initial region of two interacting parallel plane jets," Exp. Therm. Fluid Sci. **2**(4), 431–449 (1989).
[4]N. E. Bunderson and B. L. Smith, "Passive mixing control of plane parallel jets," Exp. Fluids **39**(1), 66–74 (2005).
[5]C. Soong, P. Tzeng, and C. Hsieh, "Numerical investigation of flow structure and bifurcation phenomena of confined plane twin-jet flows," Phys. Fluids **10**(11), 2910–2921 (1998).
[6]E. Tanaka, "The interference of two-dimensional parallel jets: 1st report, experiments on dual jet," Bull. JSME **13**(56), 272–280 (1970).
[7]E. Tanaka, "The interference of two-dimensional parallel jets: 2nd report, experiments on the combined flow of dual jet," Bull. JSME **17**(109), 920–927 (1974).
[8]E. Tanaka and S. Nakata, "The interference of two-dimensional parallel jets: 3rd report, the region near the nozzles in triple jets," Bull. JSME **18**(124), 1134–1141 (1975).
[9]D. Biermann and W. H. Herrnstein, *The Interference Between Struts in Various Combinations* (National Advisory Committee for Aeronautics, 1934).
[10]H. M. Spivack, "Vortex frequency and flow pattern in the wake of two parallel cylinders at varied spacing normal to an air stream," J. Aeronaut. Sci. **13**(6), 289–301 (1946).
[11]D. Sumner, S. Wong, S. Price, and M. Paidoussis, "Fluid behaviour of side-by-side circular cylinders in steady cross-flow," J. Fluids Struct. **13**(3), 309–338 (1999).
[12]P. Le Gal, M. Chauve, R. Lima, and J. Rezende, "Coupled wakes behind two circular cylinders," Phys. Rev. A **41**(8), 4566 (1990).
[13]P. Le Gal, I. Peschard, M. Chauve, and Y. Takeda, "Collective behavior of wakes downstream a row of cylinders," Phys. Fluids **8**(8), 2097–2106 (1996).
[14]M. Kiya, M. Arie, H. Tamura, and H. Mori, "Vortex shedding from two circular cylinders in staggered arrangement," J. Fluids Eng. **102**, 167 (1980).
[15]S. C. Yen and J. H. Liu, "Wake flow behind two side-by-side square cylinders," Int. J. Heat Fluid Flow **32**(1), 41–51 (2011).
[16]H. Kim and P. Durbin, "Investigation of the flow between a pair of circular cylinders in the flopping regime," J. Fluid Mech. **196**, 431–448 (1988).
[17]P. Bearman and A. Wadcock, "The interaction between a pair of circular cylinders normal to a stream," J. Fluid Mech. **61**(03), 499–511 (1973).
[18]Z. Wang and Y. Zhou, "Vortex interactions in a two side-by-side cylinder near-wake," Int. J. Heat Fluid Flow **26**(3), 362–377 (2005).
[19]M. Carini, F. Auteri, and F. Giannetti, "Secondary instabilities of the in-phase synchronized wakes past two circular cylinders in side-by-side arrangement," J. Fluids Struct. **53**, 70–83 (2015).
[20]M. Carini, F. Giannetti, and F. Auteri, "On the origin of the flip–flop instability of two side-by-side cylinder wakes," J. Fluid Mech. **742**, 552–576 (2014).
[21]M. Carini, F. Giannetti, and F. Auteri, "First instability and structural sensitivity of the flow past two side-by-side cylinders," J. Fluid Mech. **749**, 627–648 (2014).
[22]M. Hayashi, A. Sakurai, and Y. Ohya, "Wake interference of a row of normal flat plates arranged side by side in a uniform flow," J. Fluid Mech. **164**, 1–25 (1986).
[23]M. M. Alam, Y. Zhou, and X. Wang, "The wake of two side-by-side square cylinders," J. Fluid Mech. **669**, 432–471 (2011).
[24]J. Mizushima and T. Akinaga, "Vortex shedding from a row of square bars," Fluid Dyn. Res. **32**(4), 179–191 (2003).
[25]J. Mizushima and Y. Kawaguchi, "Transitions of flow past a row of square bars," J. Fluid Mech. **405**, 305–323 (2000).
[26]J. Mizushima and Y. Takemoto, "Stability of the flow past a row of square bars," J. Phys. Soc. Jpn. **65**(6), 1673–1685 (1996).
[27]Q. Zheng and M. M. Alam, "Intrinsic features of flow past three square prisms in side-by-side arrangement," J. Fluid Mech. **826**, 996–1033 (2017).
[28]M. Zdravkovich, "Review of flow interference between two circular cylinders in various arrangements," J. Fluids Eng. **99**(4), 618 (1977).
[29]A. K. M. F. Hussain, "Coherent structures and turbulence," J. Fluid Mech. **173**, 303–356 (2006).
[30]S. Chaudhuri, S. Kostka, S. G. Tuttle, M. W. Renfro, and B. M. Cetegen, "Blowoff mechanism of two dimensional bluff-body stabilized turbulent premixed flames in a prototypical combustor," Combust. Flame **158**(7), 1358–1371 (2011).
[31]B. Emerson, J. O'Connor, M. Juniper, and T. Lieuwen, "Density ratio effects on reacting bluff-body flow field characteristics," J. Fluid Mech. **706**, 219–250 (2012).
[32]S. J. Shanbhogue, S. Husain, and T. Lieuwen, "Lean blowoff of bluff body stabilized flames: Scaling and dynamics," Prog. Energy Combust. Sci. **35**(1), 98–120 (2009).
[33]C. Coats, Z. Chang, and P. Williams, "Thermoacoustic oscillations in ducted domestic heating systems," Appl. Acoust. **72**(5), 268–277 (2011).
[34]C. M. Coats, Z. Chang, and P. Williams, "Excitation of thermoacoustic oscillations by small premixed flames," Combust. Flame **157**(6), 1037–1051 (2010).
[35]W. Culler, A. Tyagi, P. Venkateswaran, and J. O'Connor, "Comparison of three interacting V-flames to a single bluff body flame at two Reynolds numbers," in *Proceedings of 54th AIAA Aerospace Sciences Meeting* (AIAA, San Diego, CA, 2016).
[36]C. H. K. Williamson, "Oblique and parallel modes of vortex shedding in the wake of a circular cylinder at low Reynolds numbers," J. Fluid Mech. **206**, 579–627 (2006).
[37]B. Cantwell and D. Coles, "An experimental study of entrainment and transport in the turbulent near wake of a circular cylinder," J. Fluid Mech. **136**, 321–374 (1983).
[38]C. H. Williamson, "Vortex dynamics in the cylinder wake," Annu. Rev. Fluid Mech. **28**(1), 477–539 (1996).
[39]S. J. Shanbhogue, *Dynamics of Perturbed Exothermic Bluff-Body Flow-Fields* (Aerospace Engineering, Georgia Institute of Technology, 2008).
[40]D.-H. Shin, *Premixed Flame Kinematics in a Harmonically Oscillating Velocity Field* (Aerospace Engineering, Georgia Institute of Technology, 2012).
[41]N. R. Lomb, "Least-squares frequency analysis of unequally spaced data," Astrophys. Space Sci. **39**, 447–462 (1976).
[42]G. Berkooz, P. Holmes, and J. L. Lumley, "The proper orthogonal decomposition in the analysis of turbulent flows," Annu. Rev. Fluid Mech. **25**(1), 539–575 (1993).
[43]D. Gabor, "Theory of communication. Part 1: The analysis of information," J. Inst. Electr. Eng.-Part III **93**(26), 429–441 (1946).
[44]B. Boashash, "Estimating and interpreting the instantaneous frequency of a signal. II. Algorithms and applications," Proc. IEEE **80**(4), 540–568 (1992).
[45]A. Prasad and C. H. Williamson, "The instability of the shear layer separating from a bluff body," J. Fluid Mech. **333**, 375–402 (1997).
[46]A. Michalke, "On spatially growing disturbances in an inviscid shear layer," J. Fluid Mech. **23**(03), 521–544 (1965).
[47]S. Aradag, S. Siegel, J. Seidel, K. Cohen, and T. McLaughlin, "Filtered POD-based low-dimensional modeling of the 3D turbulent flow behind a circular cylinder," Int. J. Numer. Methods Fluids **66**(1), 1–16 (2011).
[48]E. Mollo-Christensen, "Intermittency in large-scale turbulent flows," Annu. Rev. Fluid Mech. **5**(1), 101–118 (1973).
[49]S. J. Shanbhogue, M. Seelhorst, and T. Lieuwen, "Vortex phase-jitter in acoustically excited bluff body flames," Int. J. Spray Combust. Dyn. **1**(3), 365–387 (2009).
[50]J. Sebastian, B. Emerson, and T. Lieuwen, "Stability analysis of multiple reacting wakes," in *10th US National Combustion Meeting* (College Park, MD, 2017).
[51]L. Kabiraj and R. I. Sujith, "Nonlinear self-excited thermoacoustic oscillations: Intermittency and flame blowout," J. Fluid Mech. **713**, 376–397 (2012).
[52]H. Higuchi, J. Lewalle, and P. Crane, "On the structure of a two-dimensional wake behind a pair of flat plates," Phys. Fluids **6**(1), 297–305 (1994).
[53]B. Wieneke, "PIV uncertainty quantification from correlation statistics," Meas. Sci. Technol. **26**(7), 074002 (2015).